Research Article | Vol. 8, No. 3 | 1 Mar 2017 | BIOMEDICAL OPTICS EXPRESS 1771

Biomedical Optics EXPRESS

Multimodal nonlinear optical microscopy reveals critical role of kinesin-1 in cartilage development

SICONG HE,[1,2,6] WENQIAN XUE,[3,6] ZHIGANG DUAN,[3] QIQI SUN,[1,2] XUESONG LI,[1,2] HUIYAN GAN,[3] JIANDONG HUANG,[3,4,5,7] AND JIANAN Y. QU[1,2,8]

[1]*Department of Electronic and Computer Engineering, Hong Kong University of Science and Technology, Clear Water Bay, Kowloon, Hong Kong, China*
[2]*Center of Systems Biology and Human Health, School of Science and Institute for Advanced Study, Hong Kong University of Science and Technology, Clear Water Bay, Kowloon, Hong Kong, China*
[3]*School of Biomedical Sciences, Li Ka Shing Faculty of Medicine, The University of Hong Kong, Pok Fu Lam, Hong Kong, China*
[4]*HKU-Shenzhen Institute of Research and Innovation, Shenzhen, Guangdong, China*
[5]*Shenzhen Institute of Advanced Technologies, Shenzhen, Guangdong, China*
[6]*These authors contributed equally to this work*
[7]*jdhuang@hku.hk*
[8]*eequ@ust.hk*

Abstract: We developed a multimodal nonlinear optical (NLO) microscope system by integrating stimulated Raman scattering (SRS), second harmonic generation (SHG) and two-photon excited fluorescence (TPEF) imaging. The system was used to study the morphological and biochemical characteristics of tibial cartilage in a kinesin-1 (*Kif5b*) knockout mouse model. The detailed structure of fibrillar collagen in the extracellular matrix of cartilage was visualized by the forward and backward SHG signals, while high resolution imaging of chondrocytes was achieved by capturing endogenous TPEF and SRS signals of the cells. The results demonstrate that collagen fibrils in the superficial surface of the articular cartilage decreased significantly in the absence of *Kif5b*. The distorted morphology along with accumulated intracellular collagen was observed in the *Kif5b*-deficient chondrocytes, indicating the critical roles of kinesin-1 in the chondrocyte morphogenesis and collagen secretion. The study shows that multimodal NLO imaging method is an effective approach to investigate early development of cartilage.

OCIS codes: (170.3880) Medical and biological imaging; (180.4315) Nonlinear microscopy; (290.5910) Scattering, stimulated Raman; (170.6935) Tissue characterization.

References and links

1. J. A. Buckwalter and H. J. Mankin, "Articular cartilage: degeneration and osteoarthritis, repair, regeneration, and transplantation," Instr. Course Lect. **47**, 487–504 (1998).
2. M. B. Goldring and S. R. Goldring, "Articular cartilage and subchondral bone in the pathogenesis of osteoarthritis," Ann. N. Y. Acad. Sci. **1192**(1), 230–237 (2010).
3. H. Madry, F. P. Luyten, and A. Facchini, "Biological aspects of early osteoarthritis," Knee Surg. Sports Traumatol. Arthrosc. **20**(3), 407–422 (2012).
4. S. S. Sannasgala and D. R. Johnson, "Kinetic parameters in the growth plate of normal and achondroplastic (cn/cn) mice," J. Anat. **172**, 245–258 (1990).
5. R. Silberberg, M. Hasler, and P. Lesker, "Ultrastructure of articular cartilage of achondroplastic mice," Acta Anat. (Basel) **96**(2), 162–175 (1976).
6. A. M. Proulx and T. W. Zryd, "Costochondritis: diagnosis and treatment," Am. Fam. Physician **80**(6), 617–620 (2009).
7. B. He, J. P. Wu, T. B. Kirk, J. A. Carrino, C. Xiang, and J. Xu, "High-resolution measurements of the multilayer ultra-structure of articular cartilage and their translational potential," Arthritis Res. Ther. **16**(2), 205 (2014).
8. A. J. Sophia Fox, A. Bedi, and S. A. Rodeo, "The basic science of articular cartilage: structure, composition, and function," Sports Health **1**(6), 461–468 (2009).
9. D. Eyre, "Articular cartilage and changes in arthritis: collagen of articular cartilage," Arthritis Res. Ther. **4**, 1 (2001).

#283476 https://doi.org/10.1364/BOE.8.001771
Journal © 2017 Received 27 Dec 2016; revised 17 Feb 2017; accepted 17 Feb 2017; published 23 Feb 2017

Biomedical Optics EXPRESS

10. E. B. Hunziker, "Mechanism of longitudinal bone growth and its regulation by growth plate chondrocytes," Microsc. Res. Tech. **28**(6), 505–519 (1994).
11. L. C. Hughes, C. W. Archer, and I. ap Gwynn, "The ultrastructure of mouse articular cartilage: collagen orientation and implications for tissue functionality. A polarised light and scanning electron microscope study and review," Eur. Cell. Mater. **9**, 68–84 (2005).
12. R. Wilson, E. L. Norris, B. Brachvogel, C. Angelucci, S. Zivkovic, L. Gordon, B. C. Bernardo, J. Stermann, K. Sekiguchi, J. J. Gorman, and J. F. Bateman, "Changes in the chondrocyte and extracellular matrix proteome during post-natal mouse cartilage development," Mol. Cell. Proteomics **11,** M111.014159 (2012).
13. V. Abad, J. L. Meyers, M. Weise, R. I. Gafni, K. M. Barnes, O. Nilsson, J. D. Bacher, and J. Baron, "The role of the resting zone in growth plate chondrogenesis," Endocrinology **143**(5), 1851–1857 (2002).
14. L. J. Sandell and T. Aigner, "Articular cartilage and changes in arthritis. An introduction: cell biology of osteoarthritis," Arthritis Res. **3**(2), 107–113 (2001).
15. J. Chan, J. Huang, and K. Lai, "The kinesin motor protein KIF5B regulates RNA trafficking and dendritic spine morphologenesis in hippocampal neuron" in *Neuroscience Symposium & Annual Scientific Conference of the Hong Kong Society of Neurosciences*Anonymous (The University of Hong Kong., 2016).
16. J. Cui, Z. Wang, Q. Cheng, R. Lin, X. M. Zhang, P. S. Leung, N. G. Copeland, N. A. Jenkins, K. M. Yao, and J. D. Huang, "Targeted inactivation of kinesin-1 in pancreatic β-cells in vivo leads to insulin secretory deficiency," Diabetes **60**(1), 320–330 (2011).
17. Z. Wang, J. Cui, W. M. Wong, X. Li, W. Xue, R. Lin, J. Wang, P. Wang, J. A. Tanner, K. S. Cheah, W. Wu, and J. D. Huang, "Kif5b controls the localization of myofibril components for their assembly and linkage to the myotendinous junctions," Development **140**(3), 617–626 (2013).
18. G. Zhu, "Study of the function of Kinesin-1 (KIF5B) in long bone development," (Open Dissertation Press, 2009).
19. W. R. Zipfel, R. M. Williams, R. Christie, A. Y. Nikitin, B. T. Hyman, and W. W. Webb, "Live tissue intrinsic emission microscopy using multiphoton-excited native fluorescence and second harmonic generation," Proc. Natl. Acad. Sci. U.S.A. **100**(12), 7075–7080 (2003).
20. A. Zoumi, A. Yeh, and B. J. Tromberg, "Imaging cells and extracellular matrix in vivo by using second-harmonic generation and two-photon excited fluorescence," Proc. Natl. Acad. Sci. U.S.A. **99**(17), 11014–11019 (2002).
21. S. He, C. Ye, Q. Sun, C. K. Leung, and J. Y. Qu, "Label-free nonlinear optical imaging of mouse retina," Biomed. Opt. Express **6**(3), 1055–1066 (2015).
22. K. G. Brockbank, W. R. MacLellan, J. Xie, S. F. Hamm-Alvarez, Z. Z. Chen, and K. Schenke-Layland, "Quantitative second harmonic generation imaging of cartilage damage," Cell Tissue Bank. **9**(4), 299–307 (2008).
23. A. T. Yeh, M. J. Hammer-Wilson, D. C. Van Sickle, H. P. Benton, A. Zoumi, B. J. Tromberg, and G. M. Peavy, "Nonlinear optical microscopy of articular cartilage," Osteoarthritis Cartilage **13**(4), 345–352 (2005).
24. E. Werkmeister, N. de Isla, P. Netter, J. F. Stoltz, and D. Dumas, "Collagenous extracellular matrix of cartilage submitted to mechanical forces studied by second harmonic generation microscopy," Photochem. Photobiol. **86**(2), 302–310 (2010).
25. H. Kiyomatsu, Y. Oshima, T. Saitou, T. Miyazaki, A. Hikita, H. Miura, T. Iimura, and T. Imamura, "Quantitative SHG imaging in osteoarthritis model mice, implying a diagnostic application," Biomed. Opt. Express **6**(2), 405–420 (2015).
26. D. Fu, G. Holtom, C. Freudiger, X. Zhang, and X. S. Xie, "Hyperspectral imaging with stimulated Raman scattering by chirped femtosecond lasers," J. Phys. Chem. B **117**(16), 4634–4640 (2013).
27. S. W. Chu, S. P. Tai, T. M. Liu, C. K. Sun, and C. H. Lin, "Selective imaging in second-harmonic-generation microscopy with anisotropic radiation," J. Biomed. Opt. **14**(1), 010504 (2009).
28. R. A. R. Rao, M. R. Mehta, S. Leithem, and K. C. Toussaint, Jr., "Quantitative analysis of forward and backward second-harmonic images of collagen fibers using Fourier transform second-harmonic-generation microscopy," Opt. Lett. **34**(24), 3779–3781 (2009).
29. P. Bianchini and A. Diaspro, "Three-dimensional (3D) backward and forward second harmonic generation (SHG) microscopy of biological tissues," J. Biophotonics **1**(6), 443–450 (2008).
30. M. Han, G. Giese, and J. Bille, "Second harmonic generation imaging of collagen fibrils in cornea and sclera," Opt. Express **13**(15), 5791–5797 (2005).
31. S. P. Tai, T. H. Tsai, W. J. Lee, D. B. Shieh, Y. H. Liao, H. Y. Huang, K. Zhang, H. L. Liu, and C. K. Sun, "Optical biopsy of fixed human skin with backward-collected optical harmonics signals," Opt. Express **13**(20), 8231–8242 (2005).
32. M. Rehberg, F. Krombach, U. Pohl, and S. Dietzel, "Label-free 3D visualization of cellular and tissue structures in intact muscle with second and third harmonic generation microscopy," PLoS One **6**(11), e28237 (2011).
33. R. LaComb, O. Nadiarnykh, S. S. Townsend, and P. J. Campagnola, "Phase matching considerations in Second Harmonic Generation from tissues: Effects on emission directionality, conversion efficiency and observed morphology," Opt. Commun. **281**(7), 1823–1832 (2008).
34. M. Benjamin and J. R. Ralphs, "Fibrocartilage in tendons and ligaments--an adaptation to compressive load," J. Anat. **193**(4), 481–494 (1998).

Biomedical Optics EXPRESS

35. R. Rezakhaniha, A. Agianniotis, J. T. C. Schrauwen, A. Griffa, D. Sage, C. V. Bouten, F. N. van de Vosse, M. Unser, and N. Stergiopulos, "Experimental investigation of collagen waviness and orientation in the arterial adventitia using confocal laser scanning microscopy," Biomech. Model. Mechanobiol. **11**(3-4), 461–473 (2012).

1. Introduction

Articular cartilage is a highly specialized connective tissue covering joints. It functions as a lubricated surface for articulation by reducing friction and facilitating the transmission of loads. Study of cartilage-related diseases showed that the abnormal changes in morphology and function of cartilage are associated with various pathologies, such as osteoarthritis, achondroplasia and costochondritis [1–6]. Chondrocytes, the only resident cells in healthy cartilage, are responsible for the production and maintenance of the cartilaginous tissue. The extracellular matrix (ECM) produced by chondrocytes in the articular cartilage plays a significant role in response to tensile and compressive loadings [7]. Collagen is the most important and abundant macromolecule in the ECM of cartilage. Together with proteoglycan aggregates, the collagens facilitate the cartilage to withstand compressive forces as well as deformations. A variety of collagen types have been found in cartilage, such as type II, VI, IX and XI collagen [8]. Among these collagens, type II collagen is quantitatively dominant, accounting for 90%-95% of all the collagens in the ECM of articular cartilage [7,9]. The functions of other minor collagens are mainly to stabilize the fibril network formed by type II collagen. Disorders of ECM components may compromise the chondrocyte functions and corrupt the ECM architecture. Therefore, direct visualization of chondrocytes and collagen fibrils is of great significance to assess the health status of cartilage and to study the cartilage-related diseases.

Developing cartilage in mouse can be subdivided into six zones with unique morphologies [7,10]. The chondrocytes and ECM show distinct characteristics in different zones of cartilage. Briefly, the superficial zone (SZ), the thinnest layer with chondrocytes and collagen fibrils parallel to the articular surface, is located at the out surface of articular cartilage. In the SZ, collagen fibrils are densely packed and play biomechanical and protective roles to maintain the shear and tensile properties of articular cartilage. The middle zone, lying below the SZ, is a transitional zone in which the collagen fibrils are aligned obliquely to the articular surface and its chondrocytes demonstrate round morphologies. Next to the middle zone there is a radial zone, called the deep zone. The chondrocytes in the deep zone are well organized with the collagen fibers parallel to the chondrocyte columns and perpendicular to the articular surface. The ECM of the middle zone and deep zone (MDZ) is responsible for resisting compression [7,11]. In the growing cartilage, there exists a growth plate between the epiphysis and the metaphysis. In mammals, the elongation of longitudinal bones occurs at the growth plate by endochondral ossification. In the growth plate, there are three sub-zones: the resting zone (RZ), the proliferative zone (PZ) and the hypertrophic zone (HZ). The chondrocytes in the growth plate can be differentiated based on their specific morphologies. The chondrocytes in the RZ distribute irregularly and have a spherical appearance, and the chondrocytes in the PZ and HZ are arranged in columns, which are parallel to the long axis of the bone [12,13]. All three zones play a crucial role in endochondral bone formation, and the malfunction of the growth plate may lead to a number of disorders, such as arthritis, misshapen bones and osteochondritis dissecans [13,14].

Kinesins are a group of motor proteins responsible for directional transport along microtubules. As the most abundant kinesin motor, kinesin-1 plays a significant role in the intracellular transportation, and its functions have been studied in a variety of cells, such as neurons, pancreatic beta cells and skeletal muscle cells [15–17]. However, the roles of kinesin-1 in chondrocytes and cartilage development are still not clear. In this study, we use a kinesin-1 heavy chain (*Kif5b*) conditional knockout mouse model (*Kif5b*$^{fl/-}$*: Col2a1-Cre*) to investigate how kinesin-1 affects cartilage development. Our pilot studies have shown that *Kif5b*$^{fl/-}$*: Col2a1-Cre* mice suffer from severe chondrodysplasia [18]. Their phenotype is characterized by smaller size and shorter bones, as shown in Fig. 1.

Biomedical Optics EXPRESS

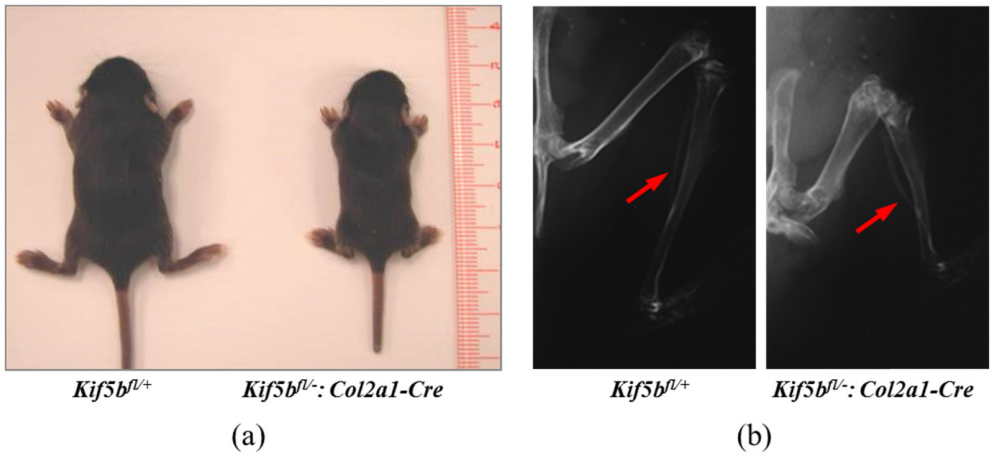

Fig. 1. (a) Representative photographs of post-natal day 10 (P10) *Kif5b*$^{fl/+}$ (left) and *Kif5b*$^{fl/-}$*: Col2a1-Cre* (right) mice. The mutant mice exhibit smaller body sizes than those of controls; (b) Representative X-ray photographs of control (left) and mutant (right) mice at six week stage. The mutant mice display shortening in femur, tibia and phalangeal bones. Arrows: tibial cortical bone.

Nonlinear optical (NLO) microscopy provides an ideal solution to resolve the structural characteristics in tissues and cells, featured with its inherent 3D resolution and capacity for deep penetration [19–21]. Recently, NLO microscopy has been used to study the chondrocytes and ECM of cartilage [22–25]. Compared with electron microscopy, a tool widely used in the study of cartilage, NLO microscopy is applicable to fresh tissues, which prevents artefacts from complicated specimen preparation. In addition, label-free imaging based on intrinsic NLO signals in the fresh biological samples provides better preservation of biological information than using fixed or frozen specimens [22]. Therefore, it is desirable to perform NLO imaging on freshly excised samples in order to accurately interpret the biomedical characteristics of tissues. In principle, the two-photon excited fluorescence (TPEF) emitted from endogenous fluorophores can facilitate label-free visualization of cellular structures; second-harmonic generation (SHG) serves as an efficient probe to view the collagenous fibrotic structure in the ECM; and stimulated Raman scattering (SRS) can be used to visualize the protein-rich structures.

In this work, we demonstrate that an integrated TPEF, SHG and SRS microscope system is capable to reveal the key morphological and biomedical characteristics of developing cartilage. Specifically, the reduced nicotinamide-adenine dinucleotide (NADH) signal was used as an endogenous fluorophore to visualize the chondrocyte morphology in different zones. Along with SRS imaging, the TPEF signals from NADH revealed the morphological alteration of chondrocytes in the *Kif5b*-deficient cartilage. The organization of collagens in the ECM were clearly depicted by both forward and backward SHG imaging, and the distribution of collagens in the articular surface of mutant cartilage was found to be substantially different from that in the control mice. Furthermore, intracellular collagen was observed in the morphologically abnormal chondrocytes, indicating misbehavior of chondrocyte secretion in the absence of *Kif5b*. The quantitative analysis of collagen structure and the morphological characterization of chondrocytes provided important insights into the roles of kinesin-1 in collagen secretion and morphogenesis of chondrocytes.

Biomedical Optics EXPRESS

2. Methods and materials

2.1 Multimodal NLO microscope system

Details of the integrated multimodal NLO microscopy system used in this work have been described in our previous study [21]. Briefly, in SRS imaging, portion of a femtosecond Ti:sapphire laser of 140 fs pulse duration (Chameleon Ultra II, Coherent, Santa Clara, CA) tuned at 830 nm was used as the pump beam. The remaining laser power (3 W) was used to pump an optical parametric oscillator (OPO) (Chameleon OPO, Coherent) to produce an infrared Stokes beam of 200 fs pulse duration at the wavelength of 1100 nm. The power of pump beam and Stokes beam on sample were 20 mW and 40 mW, respectively. The Stokes beam was modulated at 10.7 MHz by an acousto-optic modulator (3080-122, Crystal Technology). Its pulses were compressed by a prism-pair compressor before being combined with the pump beam. The differential wavenumber of the collinear pump-Stokes beams was 2957 cm^{-1}, matching to the CH_3 stretching vibrational frequency of proteins and lipids [26]. A water immersion objective (UAPON 40XW340, 1.15 NA, Olympus) was used to focus pump-Stokes beams to sample. The forward SRS signal was collected by a condenser (U-AAC, Achromat/aplanat condenser, NA 1.4, Olympus, Tokyo, Japan) and detected by a photodiode (FDS 100, Thorlabs). A high-frequency lock-in amplifier (SR844, Stanford Research Systems) was used to demodulate the SRS signal. The forward SHG (FSHG) signal excited by the Stokes beam was collected simultaneously with the SRS signal and directed to a photomultiplier tube (PMT) (H10682-210, Hamamatsu) by a dichroic mirror (760dcxru, Chroma). To excite the NADH fluorescence and backward SHG (BSHG) signals, the femtosecond laser was tuned at 780 nm. The TPEF and BSHG signals were collected by the objective and reflected to a detection system by a dichroic mirror (FF665-Di02, Semrock). The detection system of a hybrid PMT detector and a time-correlated single photon counting (TCSPC) module (HPM-100-40 and SPC-150, Becker & Hickl) was used to record time-resolved TPEF and BSHG signals sequentially by switching a pair of bandpass filters (FF02-447/60, FF01-390/40, Semrock). A pair of galvanometer scanners was used to scan the laser beams to generate SRS, SHG and TPEF images. The field of view for the multimodal images was 100 × 100 μm. The mosaic of a whole cartilage section was obtained by moving a microscope translation stage (MAX200B, Thorlabs) that holds the cartilage samples.

2.2 Cartilage specimens from mouse models

C57BL/6, *Kif5b*$^{fl/+}$ (control), and *Kif5b*$^{fl/-}$*: Col2a1-Cre* conditional knockout (mutant) mice on C57BL/6 background were used in this study. For the NLO imaging experiments, mice at different ages were sacrificed and proximal tibial heads were excised using a razor blade. The freshly dissected samples were embedded in low-melting point agarose and 150-μm-thick coronal sections were obtained by a vibratome (Vibratome 3000 Plus, The Vibratome Company). All the samples were imaged by the multimodal NLO microscope within three hours after dissected from mice. For the immunostaining experiment, hindlimbs harvested from control and mutant mice at postnatal day 15 (P15) were fixed in 4% PFA/PBS and processed for paraffin embedding. 7-um-thick coronal paraffin sections were stained according to the instruction from the manufacture of DAKO EnVision + System, Peroxidase (DAKO EnVision + System, HRP) kit. The sections were counterstained with Mayer's hematoxylin (Sigma-Aldrich). The primary antibody against *Kif5b* is homemade and has been described elsewhere [16]. The study was approved by the University of Hong Kong's Animal Ethics Committee.

Biomedical Optics EXPRESS

3. Results and discussion

3.1 Immunostaining of Kif5b in mouse tibial cartilage

To verify the inactivation efficiency of *Kif5b* in the mutant cartilage, immunostaining was performed on tibial cartilage paraffin sections obtained from P15 $Kif5b^{fl/+}$ and $Kif5b^{fl/-}$: *Col2a1-Cre* mice, respectively. As shown in Fig. 2(a), the *Kif5b* protein is expressed throughout the articular and growth plate cartilage in the control mice. In contrast, *Kif5b* signal is much weaker in the mutant group as shown in Fig. 2(b), especially in the proliferative chondrocytes. The results confirm that *Kif5b* is efficiently depleted in the growth plate chondrocytes of the $Kif5b^{fl/-}$: *Col2a1-Cre* mice. However, it is also notable that the chondrocytes in the articular cartilage maintain *Kif5b* immunoreactivity, suggesting that the depletion of *Kif5b* is not complete in the entire cartilage.

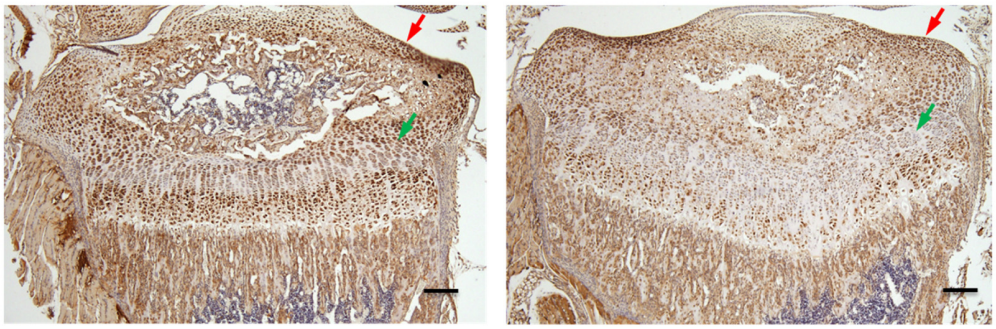

Fig. 2. Immunostaining for *Kif5b* on the tibial cartilage of the P15 mice (brown: *Kif5b* protein; blue: nuclei). (a) control mouse; (b) mutant mouse. Scale bar: 200 μm. Red arrows: articular surface. Green arrows: growth plate cartilage.

3.2 Multimodal NLO imaging of whole cartilage sections

Multimodal NLO imaging was performed to the freshly excised cartilage sections and the representative results are shown in Fig. 3. As shown in Fig. 3(a) and 3(b), the network of ECM collagen and the morphology of chondrocytes in each zone of cartilage are clearly visualized. The SRS signals of the cartilage are mainly from the proteins in chondrocytes and ECM. Peri-articular (PA) region, RZ, PZ and HZ can be clearly identified based on the morphology of protein-rich chondrocytes. The surface of this P5 articular cartilage is classified as PA region because SZ and MDZ have not fully developed and are not separable from PA. Next, the FSHG imaging shows strong SHG signals in PA zone, but not in other underlying zones, indicating that the formation of collagen network starts in the ECM of surface tissue. Apart from the SRS and FSHG signals, the TPEF signal is dominated by the endogenous fluorescence of NADH in the mitochondria of chondrocytes. Therefore, TPEF imaging serves as an additional tool to elucidate the chondrocyte morphology. As shown in the merged TPEF (green) and BSHG (red) images in Fig. 3(b), collagen networks, functioning as the supporting structure of chondrocytes, fill up the ECM throughout all zones in the cartilage. The distribution of the BSHG signal shows that it has similar features to FSHG, with strong signals from the PA region. Finally, the statistical analysis in Fig. 3(c) demonstrates that though the SHG intensity in the PA region is much stronger than other zones, the SRS signals from the ECM are homogenously distributed over the whole cartilage. This is due to that SHG source is only from the fibrillar collagen, while SRS signals come from both collagen and other protein-enriched extracellular components, such as proteoglycans. The uniform distribution of SRS signals in the whole cartilage section demonstrates that the overall protein contents in the ECM remain stable in each zone. Since

Biomedical Optics EXPRESS

the collagen network is mainly formed in articular surface, the key layer determining the biomechanical functionality of the cartilage, we performed quantitative SHG imaging in PA region (P5) and SZ (P10 and P15) to study the collagen formation in the control and *Kif5b*-depleted mutant mice.

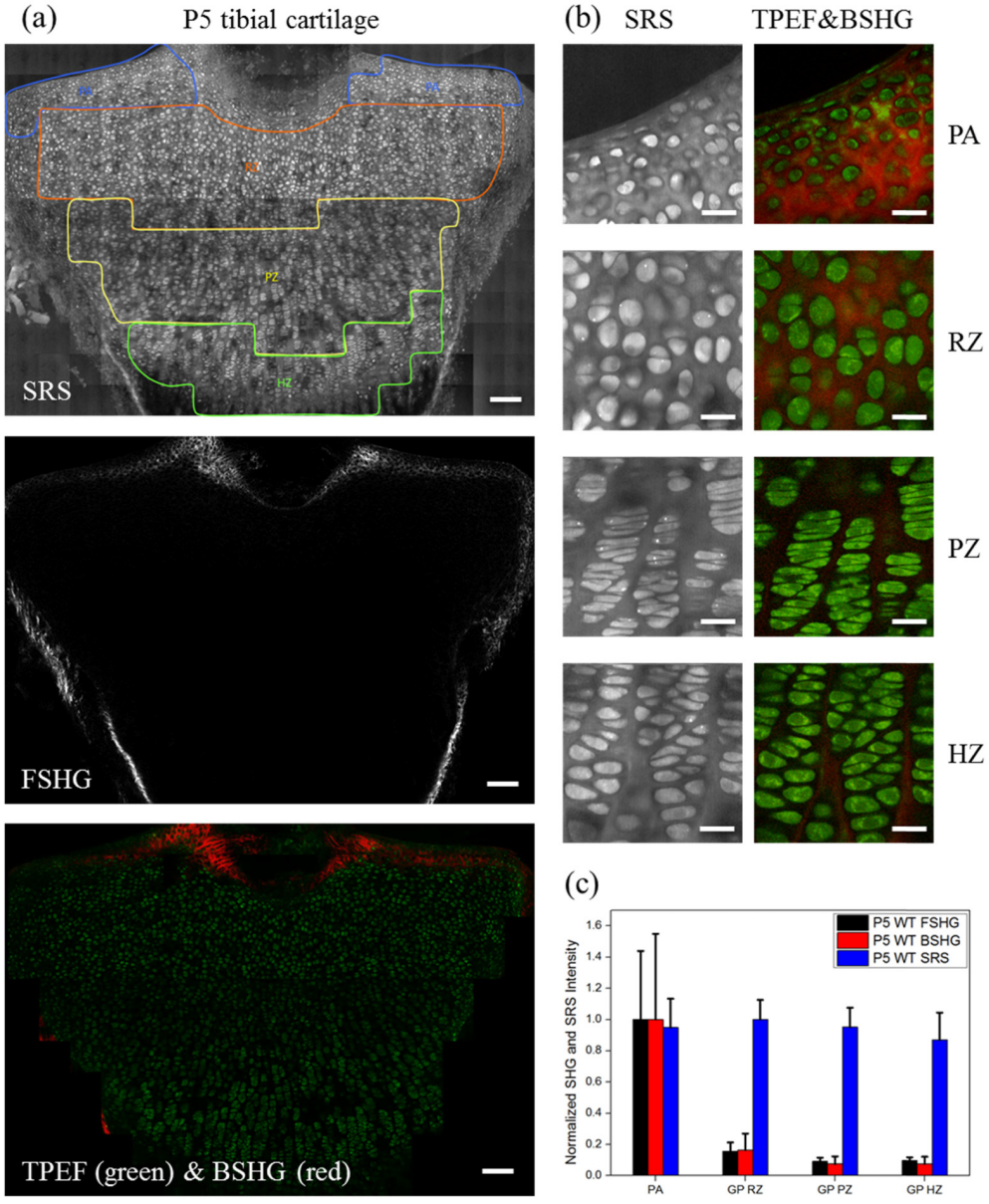

Fig. 3. Representative multimodal NLO images of tibial cartilage. (a) SRS, FSHG and TPEF&BSHG mosaics of a whole cartilage sample from a post-natal day 5 (P5) wild-type C57BL6 mouse (scale bar: 100 µm); (b) Left column: SRS images from different sub-zones in cartilage, right column: merged TPEF (green) and BSHG (red) images from corresponding zones (scale bar: 20 µm) (c) SHG and SRS intensities of the ECM in each zone calculated from 30 regions of interest in three P5 wild-type C57BL6 mice.

Biomedical Optics EXPRESS

3.3 Reduced formation of fibrillar collagen in mutant mice

To investigate the role of *Kif5b* in the development of articular surface, we performed forward and backward SHG imaging on wild-type, control and mutant mice at P5, P10 and P15 stages, respectively. As shown in Fig. 4(a) and 4(b), the representative FSHG and BSHG images from the same tissue site in SZ reveal different patterns in forward and backward directions, which is not dependent on excitation wavelength. As can be seen, though both FSHG and BSHG images show that collagen are mainly distrubted in the ECM, the detailed fibril textures of collagen can been seen in the FSHG images, while no distinct features appear in the BSHG images. This directional difference in SHG imaging has been reported in previous study of a variety of biological samples, such as muscle, cornea, skin and nerve fibers [27–32]. In theory, the directional property of SHG imaging can be explained by the quasiphasematching (QPM) condition and coherence length of SHG [27,33]. As a relaxed phase matching condition, QPM reaches the maximum conversion efficiency when the size and spacing of the collagen fibrils are in the order of the coherence length of radiation. In cartilage, the average diameter of type II collagen fibrils is within 100 nm, which is much smaller than the coherence length of FSHG. Therefore, only large fibril or densely-packed fibril bundle emits strong FSHG signal. On the other hand, BSHG has a short coherence length which is comparable to the fibril diameters of type II collagen, resulting in comparable BSHG efficiency for both large and small fibrils. Apart from fibril diameters, the inter-fibril randomness is also a crucial parameter determining the signal intensities of FSHG and BSHG. Specifically, the randomness of fibril assembly reduces the QPM effect, leading to a phenomenon that the regularly formed fibrils will have stronger FSHG than the randomly packed fibrils. Therefore, the well-formed and large collagen fibrils contribute more in FSHG signals, while BSHG signals are not sensitive to the QPM effect and signals are distributed uniformly regardless of the fibril sizes and assembly. In the study of collagen formation in the articular surface, we recorded FSHG and BSHG images from the same tissue site for analysis because they provide different information on collagen fibril structure and formation.

It should be noticed that some type I collagen enriched fibrous tissue from the ligaments connecting the center of articular cartilage emited strong SHG signals which will interfere the collection of weak type II collagen signals in SZ [34]. Therefore, the fibrous tissue was removed from all the specimens. In the analysis of SHG characteristics, we found that the signal intensity is not uniformly distrubuted over the articular surface. As can be seen from the SHG mosaic in Fig. 3(a), the SHG intensity always decays from the edge of fibrous tissue where the PA or SZ starts to the edge of articular surface. Accordingly, in this study, we measured the FSHG and BSHG signals from the entire PA (P5) and SZ (P10 and P15) to evaluate the collagen development. The resprentative distributions of SHG sginals from type II collagen over the articular surface are displayed in Fig. 4(c)-4(d). The horizontal axis is the distance from the edge of fibrous tissue marked with distinct difference in morphology and SHG pattern between the residual fibrous tissue and articular surface as shown in Fig. 3(a). As can be seen, the FSHG and BSHG distributions measured from wild-type and control mice display similar profiles at all develepmental stages from P5 to P15. The result confirms that cartilage development of the $Kif5b^{fl/+}$ control mice is similar to the wild-type mice. Therefore, the control mice can be used as good references to study the pathalogical changes in $Kif5b^{fl/-}$:*Col2a1-Cre* mutant mice. The FSHG distributions in Fig. 4(c) demonstrate that the collagen signals in mutant cartilage are similar to control at P5 and P10 stages, but suffers from severe reduction at P15. In addition, the decay profile of FSHG also disappears in mutant at P15, leaving an almost uniform distribution of collagen signal over the articular surface. On the other hand, the BSHG signals of collagen provide different information on collagen formation. As shown in Fig. 4(d), although the BSHG distribution of the mutant is similar to that of the control at P5, the distributions of BSHG from the P10 and P15 mutant display significantly lower intensity than those of the control. In particular, the difference in BSHG between mutant and control at P10 indicates that the small and randomly packed collagen

Biomedical Optics EXPRESS

fibrils are underdeveloped in the mutant. However, the similar FSHG distributions from mutant and control at P10 suggest that the large and regularly oriented collagen fibrils in the mutant are formed as normally as in control. This demonstrates that the combined FSHG and BSHG imaging provides crucial insight into the effect of *Kif5b* on the formation of collagen fibrils in articular surface. Overall, the results indicate that there is no significant difference in collagen synthesis in PA between mutant and control at P5 stage. With further development to P10, the formation of randomly oriented small fibrils in mutant SZ starts to retard in comparison with control, while the fomration of large and regularly orientted fibrils remains normal. At P15 stage, the contents of both types of collagen fibrils in mutant are lower than control. Since the biomechanical functionality of the cartilage is stronlgy associated with the collagen formation in articular surface, the significant deficiency of collagen in the mutant may lead to potential dysfunction of the cartilage in the *Kif5b*-depleted mice.

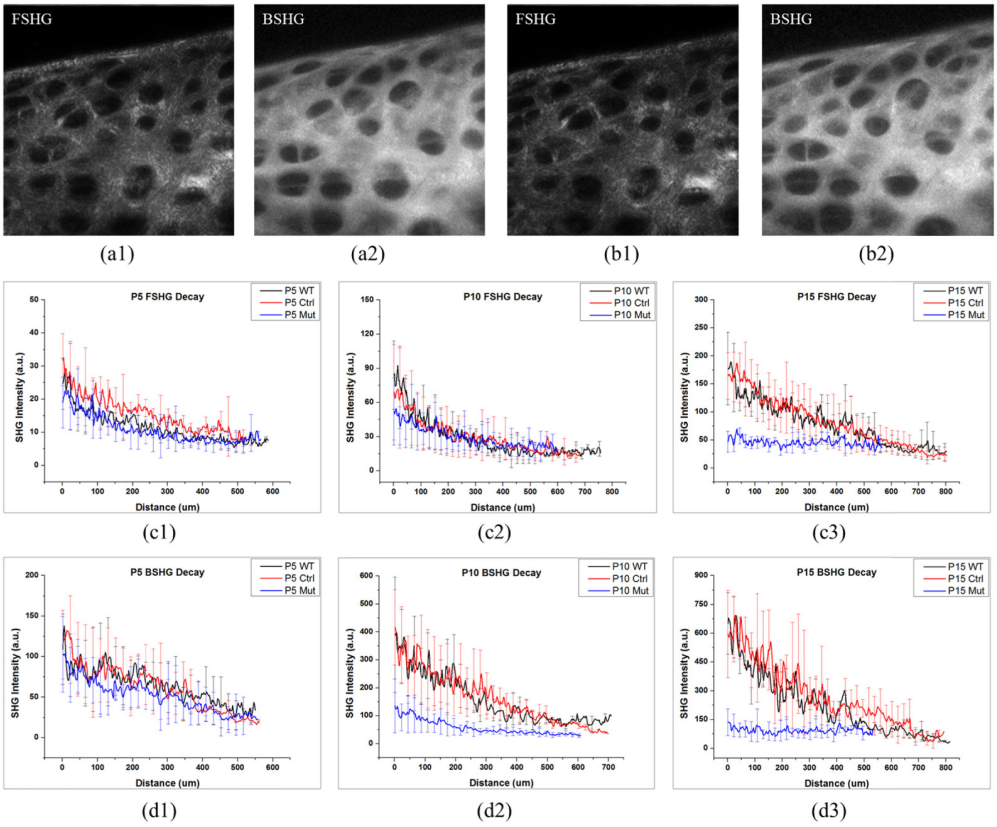

Fig. 4. Representative FSHG and BSHG signals in the PA and SZ of articular cartilage in wild-type, control and mutant mice. (a1)-(a2) FSHG and BSHG images of SZ from a P15 control mouse (excitation: 780 nm; field of view: 100 µm × 100 µm); (b1)-(b2) FSHG and BSHG images of SZ from a P15 control mouse (excitation: 1100 nm; field of view: 100 µm × 100 µm); (c) FSHG signal distributions at P5, P10 and P15 stages from wild-type (WT), control (Ctrl) and mutant (Mut) mice; (d) BSHG signal distributions at P5, P10 and P15 stages from wild-type (WT), control (Ctrl) and mutant (Mut) mice. Each statistical distribution curve in (c)-(d) is shown in terms of average with standard deviation over the measurements from six specimens.

3.4 Distorted morphology of chondrocytes in mutant mice

Apart from collagen formation in the ECM of articular surface, we studied the morphology of chondrocytes in the cartilages of control and mutant mice. Here the endogenous NADH fluorescence was used to visualize the morphological features of chondrocytes. The

Biomedical Optics EXPRESS

representative TPEF images in Fig. 5 display the morphology of chondrocytes in different zones of control and mutant cartilages at P5, P10 and P15 stages. In a comparison of control with mutant cartilage, the morphology of chondrocytes in the mutant is significantly distorted. Particularly, the columnar structures of a normal growth plate are replaced by randomly arranged chondrocytes in the mutant cartilage. It is also noted that the abnormal morphology of chondrocytes occurs in the mutant at P5 and becomes severe at P10 and P15. Considering that the columnar arrangement of chondrocytes in the growth plate is crucial for bone formation, the disorganization of chondrocytes in the mutant cartilage may be associated with the retarded growth of bone as shown in Fig. 1(b). The distorted morphology mainly appears in the growth plate of cartilage, not in the articular surface, such as PA and SZ. This is due to that the depletion efficiency of *Kif5b* in the growth plate is higher than that in articular cartilage, as indicated in the results of immunostaining study shown in Fig. 2.

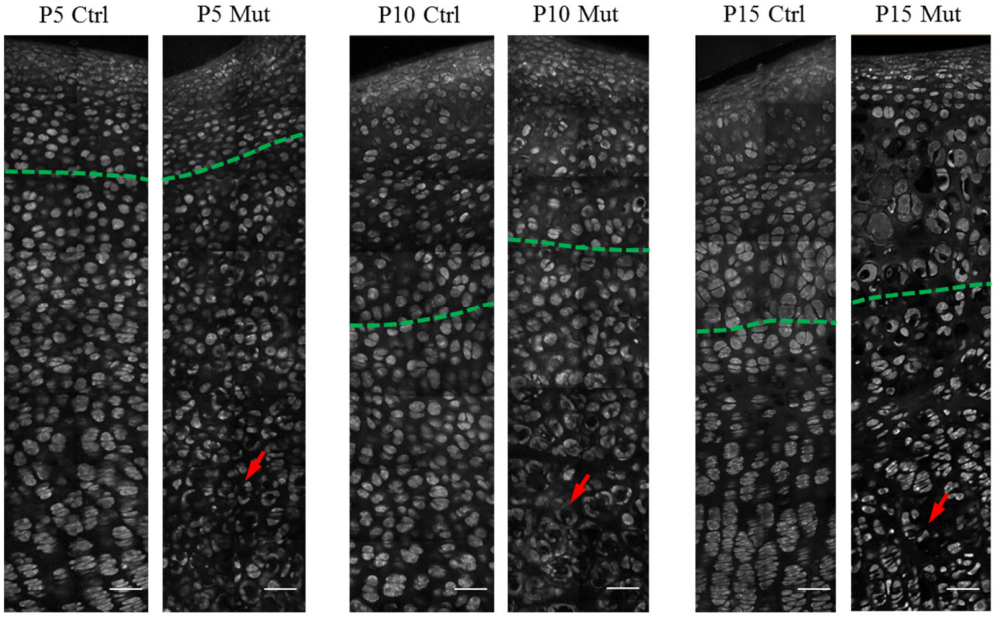

Fig. 5. Representative TPEF mosaics of control and mutant cartilage at P5, P10 and P15 (scale bar: 50 μm). Green dashed lines: the boundary between articular cartilage and growth plate cartilage. Red arrows: distorted chondrocytes in the growth plate of mutant cartilages.

An astonishing finding is that we observed intracellular collagen in the morphologically distorted chondrocytes of P15 mutant cartilage. As shown in Fig. 6(a), the intracellular collagen is mainly distributed in the abnormal chondrocytes in MDZ and generates SHG signals stronger than the surrounding ECM. The details of an abnormal chondrocyte with intracellular collagen are shown in Fig. 6(b). The SHG image demonstrates that the majority of intracellular volume is filled up with the collagen. Since intracellular collagen was not observed in wide-type and control cartilage, the accumulation of intracellular collagen must be associated with abnormal secretion of collagen in the *Kif5b*-depleted chondrocytes. Next, we performed texture analysis on SHG images of MDZ to characterize the intracellular collagen and the collagen fibrils in the surrounding ECM. The spatial coherency value, an indicator representing the overall spatial isotropy of textures, was used for quantitative analysis on the texture of SHG images. The coherency values of the collagen fibrils in the SHG images were calculated by OrientationJ, an ImageJ's plug-in. OrientationJ evaluates the isotropic properties of every pixel in the region of interest, and it has been widely used to analyze biomedical images [35]. In OrientationJ, coherency values are bounded between 0 and 1, with 0 indicating isotropic structures and 1 indicating that the fibrils are well arranged

Biomedical Optics EXPRESS

along one dominant direction. As shown in Fig. 6(c), the coherency values of the intracellular collagen are significantly higher than those of extracellular collagen in both FSHG and BSHG images, suggesting that the intracellular collagen fibrils are more oriented and have a low isotropy. It should be emphasized that the intracellular collagen was mainly found in mutant cartilages at P15, rather than P5 and P10. The discovery of distorted morphology of chondrocytes and accumulated intracellular collagen in the mutant cartilage indicates that kinesin-1 may play a significant role in maintaining the integrity of chondrocyte morphogenesis and collagen secretion in cartilage.

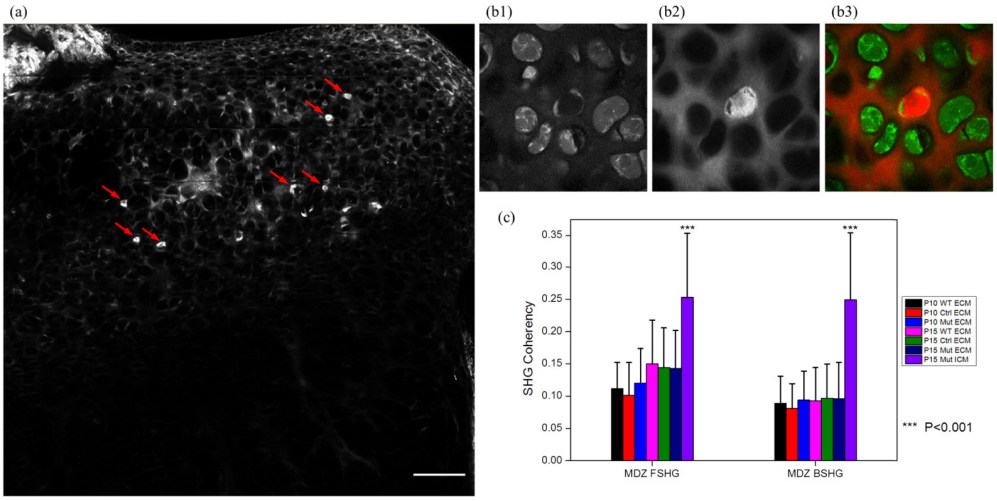

Fig. 6. Accumulated intracellular collagen in mutant cartilage. (a) Representative FSHG mosaic of P15 mutant cartilage section (scale bar: 100 μm). Intracellular collagen is highlighted by strong SHG signal (red arrows); (b) Representative TPEF image (b1), BSHG image (b2) and merged image (b3) of a region with accumulated intracellular collagen (field of view: 100 μm × 100 μm); (c) Coherency values calculated from the FSHG and BSHG of the MDZ of P10 and P15 mice from 30 sites (3 mice for each group). ICM: intracellular matrix.

4. Conclusion

In this study, we have demonstrated that multimodal label-free NLO microscopy is a powerful tool to investigate the developmental defects of cartilage in *Kif5b* knockout mice. High-resolution label-free visualization of chondrocytes in each zone of cartilage can be achieved by SRS and TPEF imaging based on the vibrational signals of proteins and endogenous fluorescence of NADH, respectively. The distorted morphology of chondrocytes and loss of columnar arrangement in the growth plate of mutant cartilage reveal potentially profound effect of *Kif5b* depletion on early development of bones. In the PA (P5) and SZ (P10 and P15) of articular cartilage, fine structures of type II collagen in the ECM can be clearly resolved by SHG imaging. The combined FSHG and BSHG imaging provides quantitative information on the formation of collagen networks in early cartilage development. The results show that there is no significant difference in collagen synthesis in PA between mutant and control at P5 stage. However, the formation of randomly oriented small fibrils in mutant SZ start to retard in comparison with control at P10, while the formation of large and regularly oriented fibrils remains normal. At P15 stage, the contents of large and small collagen fibrils in mutant were much lower than control. It should be pointed out that though the ECM malformation was revealed in PA and SZ of mutant cartilage by the combined FSHG and BSHG imaging, the chondrocytes display normal morphology in the zones. This suggests that the imaging technique may detect ultrastructural abnormality in ECM prior to the morphological alteration of cells. Furthermore, we observed the accumulation of intracellular collagens in the MDZ of the mutant cartilage at P15, indicating

Biomedical Optics EXPRESS

abnormal secretion of collagen from the chondrocytes in absence of *Kif5b*. The results of this work show that multimodal NLO microscopy offers a unique approach to study the pathological characteristics of biological tissues. The label-free NLO imaging is of great advantage to preserve their intrinsic information and enable quantitative analysis of their structure and biochemistry at sub-cellular level.

Funding

Hong Kong Research Grants Council through grants 662513, 16103215, 16148816, 768113M, 17127015, T13-607/12R, T13-706/11-1 and T12-708/12-N, AOE/M-09/12, AOE/M-04/04, a 973 grant (2014CB745202) from the Ministry of Science and Technology of PRC, and by Shenzhen Peacock project (KQTD2015033117210153), Shenzhen Science and Technology Innovation Committee Basic Science Research Grant (JCYJ20150629151046896), NSF of Guangdong Province Grant (2015A030313745), and Hong Kong University of Science & Technology (HKUST) through grant RPC10EG33.